JCTC Journal of Chemical Theory and Computation

Density Functional Theory Study of the Formation of Naphthalene and Phenanthrene from Reactions of Phenyl with Vinyl- and Phenylacetylene

Jorge Aguilera-Iparraguirre and Wim Klopper*

Lehrstuhl für Theoretische Chemie, Institut für Physikalische Chemie, Universität Karlsruhe (TH), D-76128 Karlsruhe, Germany

Received August 7, 2006

Abstract: Reaction pathways for polycyclic aromatic hydrocarbon growth from reactions of either vinyl- or phenylacetylene with a phenyl radical are proposed and investigated using density functional theory (DFT). B3LYP/TZVP calculations are performed to obtain structures of minima and saddle points as well as kinetic data, supplemented with BMK/TZVP single-point energy calculations. The pathways include a cis−trans isomerization via a radicalic four-membered ring intermediate, which has so far not been considered in the literature. The DFT approach is validated against coupled-cluster calculations of a model system representing this intermediate. The coupled-cluster calculations include single and double excitations as well as perturbative corrections for connected triples and are performed in a correlation-consistent cc-pVTZ basis.

I. Introduction

The chemical vapor deposition (CVD) of carbon from light hydrocarbons involves a large and complex set of homogeneous gas-phase reactions leading to various products including polycyclic aromatic hydrocarbons (PAHs) and heterogeneous surface reactions leading to the deposition of pyrolytic carbon on the substrate.[1−3] Recently, Norinaga et al. studied the product distributions in the CVD of carbon from acetylene at 8 kPa and 900 °C and found that the major products formed under these conditions are benzene, dihydrogen, vinylacetylene, naphthalene, ethylene, and methane.[4] Benzene and vinylacetylene are known to be formed in acetylene pyrolysis, and in ref 4, it was suggested that vinylacetylene is formed by the dimerization of acetylene while benzene is formed by the combination of acetylene and vinylacetylene. Possible reactions for benzene formation from small aliphatics are

$$n\text{-}C_4H_3 + C_2H_2 \rightarrow \text{phenyl} \quad (1)$$

$$n\text{-}C_4H_5 + C_2H_2 \rightarrow \text{benzene} + H \quad (2)$$

$$C_3H_3 + C_3H_3 \rightarrow \text{benzene} \quad (3)$$

Although still under debate (cf. refs 5−7 for a review of the literature), we shall in this article not be concerned with the formation of benzene but rather with the formation of larger PAHs such as naphthalene and phenanthrene.

The addition of vinylacetylene to benzene (or more precisely phenyl) is a possible route to naphthalene formation:[8]

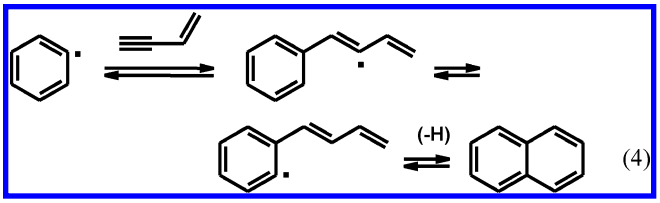

(4)

While Appel and co-workers have reported that, in their kinetic modeling, the vinylacetylene addition channel (eq 4) contributed the most to the naphthalene production,[8] Frenklach and others have argued that eq 4 may be ineffective because of the large barrier to rotation about the C=C double bond in the last step.[5,9,10]

Appel and co-workers have furthermore suggested that phenanthrene is formed primarily via ring−ring condensation reactions, such as

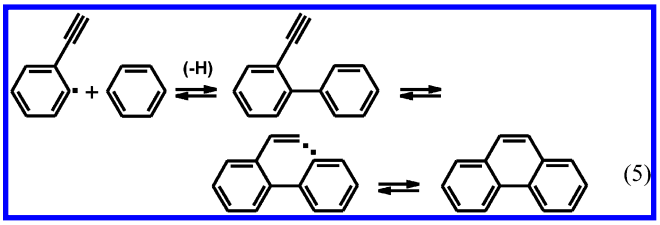

(5)

* Corresponding author fax: +49-721-608-3319; e-mail: klopper@chem-bio.uni-karlsruhe.de.

10.1021/ct600255u CCC: $37.00
Published on Web 12/08/2006

Table 1. Parameters Used in the Kinetic Modeling in ref 13

reaction	A (cm^3 mol^{-1} s^{-1})	n	E_a (kJ mol^{-1})	ref
phenyl + vinylacetylene → naphthalene + H	9.900×10^{30}	−5.07	88.29	8
phenyl + phenylacetylene → phenanthrene + H	9.550×10^{11}	0.0	18.03	6

Alternatively, the growth of phenanthrene could be initiated by the formation of biphenyl from benzene, then yielding phenanthrene via the HACA mechanism (hydrogen-abstraction−C_2H_2-addition) of Frenklach and Wang.[5,11,12]

In their kinetic modeling of acetylene pyrolysis (900 °C, 8 kPa, and 0.5 s), Norinaga and Deutschmann[13,14] found that 68% of acetylene is consumed by dimerization to form vinylacetylene ($2C_2H_2 \rightarrow C_4H_4$), 17% by diacetylene formation ($2C_2H_2 \rightarrow C_4H_2 + H_2$), and 7% by benzene formation from vinylacetylene and acetylene ($C_4H_4 + C_2H_2 \rightarrow$ benzene). From the viewpoint of the products, 98% of vinylacetylene is formed by the dimerization of acetylene, and 95% of benzene is formed by the combination of vinylacetylene and acetylene.

In ref 13, modeling was performed with a mechanism involving 227 species and 827 reactions. In the present work, we shall concentrate on two of these reactions that seem to play an important role in the formation of larger PAHs. In ref 4, for example, yields (based on C_1) of ca. 2% of naphthalene and ca. 1% of phenanthrene were observed in acetylene pyrolysis after about 1.0 s under the aforementioned conditions.

The kinetic modeling of ref 13 was based on Arrhenius-like rate expressions:

$$k(T) = AT^n \exp(-E_a/RT) \tag{6}$$

with the kinetic parameters (pre-exponential A, temperature exponent n, activation energy E_a) taken from the literature (R is the gas constant and T is the temperature). Because the modeling of the formation of naphthalene and phenanthrene appeared to be difficult, we decided to reinvestigate—by means of density functional theory (DFT)—the two sets of parameters shown in Table 1. We shall show in this article that very different parameters can be derived from a reaction mechanism that involves a cis−trans isomerization via a radicalic four-membered ring, which has so far not been considered in the literature:

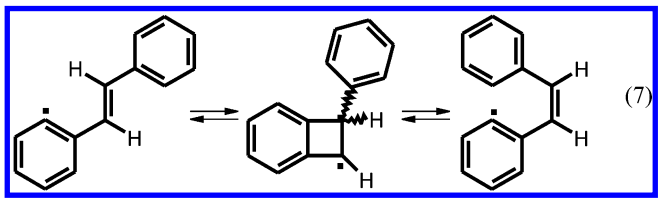

(7)

The present study describes the DFT investigations of the reactions of phenyl with vinylacetylene and phenylacetylene via this four-membered intermediate.

II. Computational Section

Geometry optimizations utilizing analytic nuclear gradients were carried out to locate minima and saddle points using DFT methods as implemented in the Turbomole program package.[15−18] At the initial stage of our work, we used the SV(P) basis[19,20] (split-valence basis with a set of d-type polarization functions on C) and the BP86 functional[21−23] in combination with the RI-J approximation[24,25] to explore possible pathways at a very low computational cost. The RI-J approximation reduces the computing time to about 10% of the time needed for the corresponding calculation without this approximation.

Subsequently, the final results were obtained by locating the minima and saddle points using the TZVP basis[20,26] (triple-ζ valence plus polarization) and the B3LYP functional.[22,27,28] Moreover, single-point calculations were carried out in the same TZVP basis using the BMK functional,[29] which has been designed specifically for accurate calculations of barrier heights. The RI-J approximation was not invoked in the B3LYP and BMK calculations. Redundant internal coordinates were used in the geometry optimizations,[30] and the optimization of saddle points was performed using the TRIM method (trust radius image minimization).[31] Harmonic frequencies were calculated for all species at the B3LYP/TZVP level.[32,33] The frequencies of the minima were all real, and the saddle points exhibited only one imaginary frequency. The harmonic frequencies were scaled by a factor of 0.9 and used to compute the zero-point vibrational energies (ZPVE) and vibrational partition functions.

Simple transition state theory (TST) was used to compute reaction rate constants. This theory assumes that the reaction rate is limited by the formation of the transition state, which is considered to be in pseudo-equilibrium with the reactants. The reaction rate constants can be calculated from the thermochemistry of reactants and transition states, that is, by calculating translational, rotational, and vibrational partition functions. In these calculations, the imaginary frequency of the transition structure is ignored and only $3N - 7$ molecular vibrations remain (for a nonlinear molecule).

The expression for the reaction rate constant of a unimolecular reaction is

$$k(T) = \kappa(T)\frac{k_B T}{h}\frac{Q^{\ddagger}_{int}(T)}{Q^{R}_{int}(T)}\exp(-E_a/RT) \tag{8}$$

where $Q^{\ddagger}_{int}$ and Q^{R}_{int} are the partition functions of the transition state and reactants respectively, involving only internal coordinates, and calculated using the module Freeh, available in Turbomole. k_B is the Boltzmann constant and h the Planck constant. The temperature T is varied from 300 to 1300 K in the present work. E_a is the barrier height including ZPVE. $\kappa(T)$ is the transmission coefficient accounting for tunneling effects, computed in the present work from the formula[34]

$$\kappa(T) = 1 - \frac{1}{24}\left(\frac{h\upsilon^{\ddagger}}{k_B T}\right)^2\left(1 + \frac{RT}{E_a}\right) \tag{9}$$

Only the imaginary frequency associated with the reaction

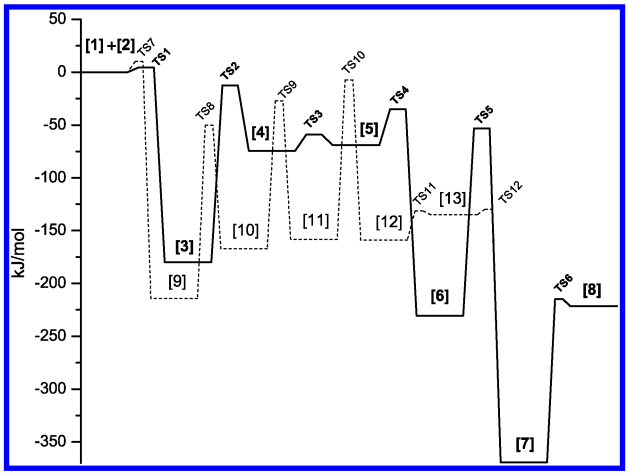

Figure 1. Formation of naphthalene, C_6H_5 [**1**] + C_4H_4 [**2**] → $C_{10}H_{10}$ [**8**], calculated at the B3LYP/TZVP level.

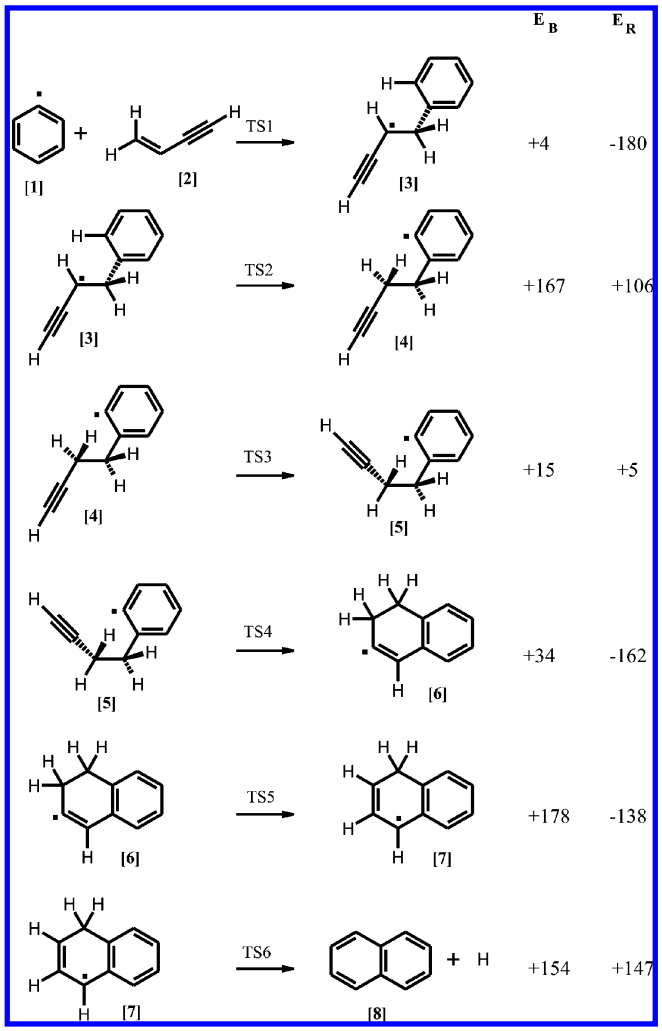

Figure 2. Intermediates and transition states on the first reaction path (solid line in Figure 1) toward the formation of naphthalene, C_6H_5 [**1**] + C_4H_4 [**2**] → $C_{10}H_{10}$ [**8**], calculated at the B3LYP/TZVP level (electronic energies in kJ/mol).

coordinate $\upsilon^{\ddagger}$ is required to calculate $\kappa(T)$. Notice that the minus sign of the second term on the right-hand side of eq 9 is cancelled by the square of the imaginary frequency $\upsilon^{\ddagger}$, such that $\kappa(T) > 1$.

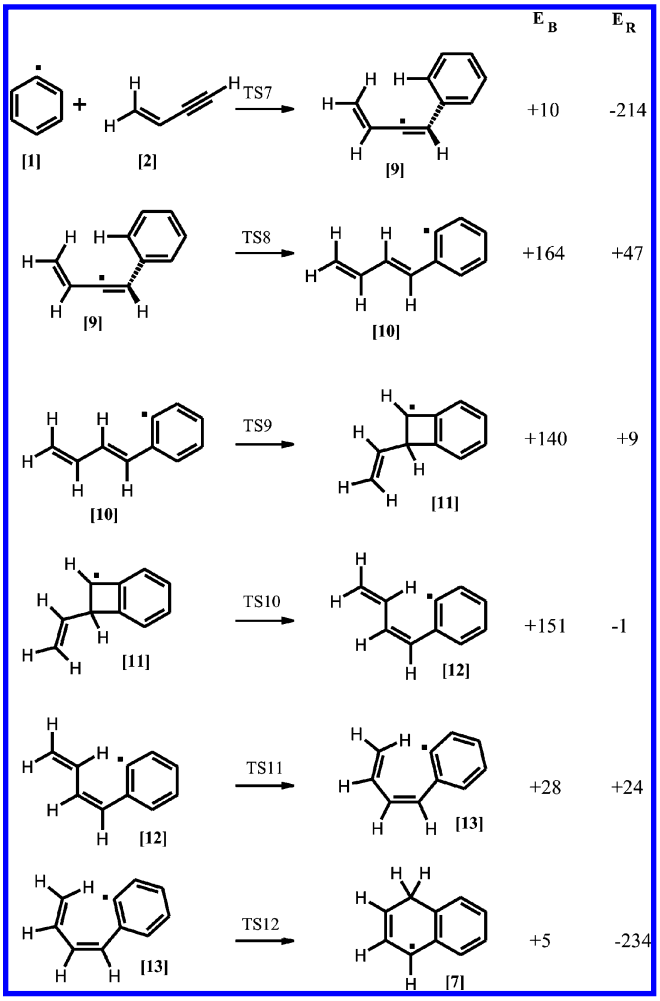

Figure 3. Intermediates and transition states on the second reaction path (dashed line in Figure 1) toward the formation of naphthalene, C_6H_5 [**1**] + C_4H_4 [**2**] → $C_{10}H_{10}$ [**8**], calculated at the B3LYP/TZVP level (electronic energies in kJ/mol).

For a bimolecular reaction, the expression for the reaction rate constant is

$$k(T) = \kappa(T)\,\bar{V}(T)\frac{k_B T}{h}\frac{Q^{\ddagger}(T)}{Q^{R_1}(T)Q^{R_2}(T)}\exp(-E_a/RT) \quad (10)$$

where $Q^{\ddagger}(T)$, $Q^{R_1}(T)$ and $Q^{R_2}(T)$ are the partition functions (including translation) of the activated complex and the two reactants R_1 and R_2, respectively, and $\bar{V}(T)$ is the molar volume of an ideal gas at temperature T.

Arrhenius-like expressions (eq 6) are fitted to the computed rate constants for a series of temperatures in the range from 300 to 1300 K, treating A and n as fitting parameters. E_a is taken as the energy difference (including ZPVE) between the transition state and reactants, and this energy difference is taken directly from the DFT calculation. If necessary, it could be replaced with a more accurate value, for example, from advanced coupled-cluster single-point calculations at the DFT geometries. We have performed single-point calculations with the functional BMK at the B3LYP geometries to obtain good estimates of E_a. It has been shown before that the BMK functional,[29,35] which has been designed and parametrized for kinetics, yields more reliable barrier

Table 2. Calculated TST Rate Constants for the Formation of Naphthalene

	T							
reaction	300	400	500	600	700	800	900	1000
1 + **2** → **3**[a]	5.94×10^{-15}	2.08×10^{-14}	5.23×10^{-14}	1.06×10^{-13}	1.90×10^{-13}	3.12×10^{-13}	4.73×10^{-13}	6.93×10^{-13}
3 → **4**[b]	4.16×10^{-16}	2.34×10^{-9}	2.58×10^{-5}	1.28×10^{-2}	1.07×10^{0}	3.03×10^{1}	4.13×10^{2}	3.32×10^{3}
4 → **5**[b]	1.28×10^{10}	5.95×10^{10}	1.52×10^{11}	2.79×10^{11}	4.33×10^{11}	6.04×10^{11}	7.80×10^{11}	9.57×10^{11}
5 → **6**[b]	8.43×10^{5}	2.11×10^{7}	1.43×10^{8}	5.32×10^{8}	1.32×10^{9}	2.66×10^{9}	4.60×10^{9}	7.13×10^{9}
6 → **7**[b]	8.81×10^{-16}	1.06×10^{-8}	1.91×10^{-4}	1.32×10^{-1}	1.45×10^{1}	4.94×10^{2}	7.86×10^{3}	7.19×10^{4}
7 → **8** + H[b]	8.74×10^{-12}	1.00×10^{-5}	4.67×10^{-2}	1.33×10^{1}	7.84×10^{2}	1.70×10^{4}	1.87×10^{5}	1.31×10^{6}
1 + **2** → **9**[a]	8.02×10^{-15}	4.87×10^{-14}	1.68×10^{-13}	4.25×10^{-13}	8.72×10^{-13}	1.62×10^{-12}	2.68×10^{-12}	4.23×10^{-12}
9 → **10**[b]	1.28×10^{-14}	5.06×10^{-8}	4.38×10^{-4}	1.85×10^{-1}	1.40×10^{1}	3.61×10^{2}	4.51×10^{3}	3.49×10^{4}
10 → **11**[b]	6.55×10^{-12}	5.36×10^{-6}	1.91×10^{-2}	4.47×10^{0}	2.29×10^{2}	4.34×10^{3}	4.26×10^{4}	2.66×10^{5}
11 → **12**[b]	2.18×10^{-13}	6.29×10^{-7}	4.78×10^{-3}	1.84×10^{0}	1.30×10^{2}	3.25×10^{3}	3.97×10^{4}	2.88×10^{5}
12 → **13**[b]	8.54×10^{7}	1.23×10^{9}	6.28×10^{9}	1.82×10^{10}	3.92×10^{10}	7.00×10^{10}	1.09×10^{11}	1.60×10^{11}
13 → **7**[b]	5.23×10^{11}	9.74×10^{11}	1.53×10^{12}	2.13×10^{12}	2.79×10^{12}	3.48×10^{12}	4.19×10^{12}	4.92×10^{12}

	T			fit: $AT^n \exp(-E_a/RT)$			
reaction	1100	1200	1300	*A*	*n*	E_a^{B3LYP}	E_a^{BMK} [c]
1 + **2** → **3**[a]	9.71×10^{-13}	1.28×10^{-12}	1.70×10^{-12}	2.09×10^{-20}	2.61	6.0	6.9
3 → **4**[b]	1.86×10^{4}	7.82×10^{4}	2.62×10^{5}	2.53×10^{13}	−0.55	157.0	157.4
4 → **5**[b]	1.13×10^{12}	1.33×10^{12}	1.49×10^{12}	2.71×10^{12}	0.11	14.8	15.3
5 → **6**[b]	1.00×10^{10}	1.34×10^{10}	1.72×10^{10}	6.85×10^{11}	−0.10	32.5	34.2
6 → **7**[b]	4.43×10^{5}	2.04×10^{6}	7.38×10^{6}	1.05×10^{13}	0.10	162.1	170.9
7 → **8** + H[b]	6.31×10^{6}	2.37×10^{7}	7.40×10^{7}	1.97×10^{10}	0.97	135.8	146.3
1 + **2** → **9**[a]	6.18×10^{-12}	8.62×10^{-12}	1.19×10^{-11}	1.07×10^{-19}	2.72	10.7	13.4
9 → **10**[b]	1.84×10^{5}	7.48×10^{5}	2.46×10^{6}	1.19×10^{14}	−0.51	152.8	157.7
10 → **11**[b]	1.20×10^{6}	4.23×10^{6}	1.21×10^{7}	5.54×10^{11}	0.23	134.4	135.9
11 → **12**[b]	1.48×10^{6}	5.75×10^{6}	1.82×10^{7}	7.00×10^{11}	0.41	145.7	177.3
12 → **13**[b]	2.13×10^{11}	2.72×10^{11}	3.38×10^{11}	8.85×10^{11}	0.20	25.7	22.5
13 → **7**[b]	5.65×10^{12}	6.47×10^{12}	7.23×10^{12}	1.49×10^{10}	0.91	4.2	4.0

[a] In $cm^3\ s^{-1}$ molecule^{-1}, with *T* in K and E_a in kJ/mol. [b] In s^{-1}, with *T* in K and E_a in kJ/mol. [c] This value includes a ZPVE correction calculated at the B3LYP level.

heights than B3LYP (but not necessarily more accurate geometries or vibrational frequencies).

Parts of the pathways were investigated with a variety of different functionals in order to assess the accuracy of the BMK results. Single-point calculations (at the B3LYP/TZVP geometries) were performed with the functionals BLYP,[28] TPSS,[36,37] TPSSh,[36−38] and B97-K.[29] It turned out that the computed energies were quite different for the four-membered ring intermediate, and we therefore studied the isomerization of the penta-1,3-dien-1-yl radical [**21**] as a model for the formation of this intermediate, using the MP2,[39] CC2,[40] and RCCSD(T)[41−43] methods, the latter as implemented in the Molpro[44−46] program package. The MP2 and CC2 calculations were performed with the Turbomole[15] program using the resolution-of-the-identity approximation.[39,40] The innershell electrons (carbon 1s) were not correlated (frozen core, FC, approximation) in any of the correlation treatments.

III. Results and Discussion

A. Formation of Naphthalene. We have computed two pathways for the formation of naphthalene from phenyl and vinylacetylene. On one pathway, the phenyl radical attacks the vinylacetylene at its double bond (solid line in Figure 1, see also Figure 2), and on the other pathway, the phenyl radical attacks the vinylacetylene at its triple bond (dashed line in 1, see also Figure 3). The attack at the double bond yields [**3**] and is followed by a 1,4 hydrogen shift, bringing the radical center back to the ring ([**4**]). Then, further reactions to naphthalene ([**8**]) are straightforward. The other possible pathway occurs after the phenyl's attack of the triple bond of vinylacetylene, yielding [**9**]. Here also, a 1,4 hydrogen shift brings the radical center back to the ring ([**10**]). To proceed further, a rotation about a double bond seems required to prepare for the closure of the second six-ring of naphthalene, and it was this rotation about a double bond that, in previous work, let the second pathway seem inefficient, because barriers to rotation about a double bond are usually very high.[5,9,10]

In our study, however, this rotation takes place in a two-step reaction via the intermediate [**11**]. This four-membered ring helps to decrease the barrier to "rotation" about the double bond significantly. From [**12**] onwards, the ring closure to yield naphthalene is straightforward. We stress that, in contrast to the work by Moriarty and Frenklach,[9] we do not find any structure (minimum or saddle point) with an electronic energy above the transition state of the first, bimolecular reaction step (TS1 or TS7, cf. Figure 1).

In Table 2, we provide the reaction rates obtained from TST for all of the steps of the two pathways in the temperature range 300−1300 K, along with the fitted Arrhenius parameters *A* and *n* and computed values of E_a (including ZPVE). We give the activation energies obtained from calculations with the density functionals B3LYP and

Table 3. Calculated TST Rate Constants for the Formation of Phenanthrene

	T							
reaction	300	400	500	600	700	800	900	1000
1 + **14** → **15**[a]	3.83×10^{-15}	2.65×10^{-14}	9.87×10^{-14}	2.61×10^{-13}	5.57×10^{-13}	1.06×10^{-12}	1.79×10^{-12}	2.80×10^{-12}
15 → **16**[b]	8.02×10^{-13}	1.00×10^{-6}	4.49×10^{-3}	1.21×10^{0}	6.59×10^{1}	1.35×10^{3}	1.43×10^{4}	9.51×10^{4}
16 → **17**[b]	1.11×10^{-10}	3.23×10^{-5}	6.18×10^{-2}	9.57×10^{0}	3.55×10^{2}	5.39×10^{3}	4.45×10^{4}	2.46×10^{5}
17 → **18**[b]	1.80×10^{-15}	1.65×10^{-8}	2.49×10^{-4}	1.54×10^{-1}	1.53×10^{1}	4.87×10^{2}	7.17×10^{3}	6.18×10^{4}
18 → **19**[b]	6.17×10^{8}	2.80×10^{9}	7.07×10^{9}	1.31×10^{10}	2.02×10^{10}	2.87×10^{10}	3.73×10^{10}	4.64×10^{10}
19 → **20** + H[b]	5.70×10^{-2}	2.03×10^{2}	2.91×10^{4}	8.36×10^{5}	9.50×10^{6}	5.85×10^{7}	2.49×10^{8}	7.96×10^{8}

	T			fit: $AT^n \exp(-E_a/RT)$			
reaction	1100	1200	1300	*A*	*n*	E_a^{B3LYP}	E_a^{BMK} [c]
1 + **14** → **15**[a]	4.27×10^{-12}	6.02×10^{-12}	8.30×10^{-12}	6.96×10^{-20}	2.74	11.8	14.7
15 → **16**[b]	4.51×10^{5}	1.63×10^{6}	4.89×10^{6}	8.82×10^{13}	−0.51	141.8	142.8
16 → **17**[b]	9.67×10^{5}	3.12×10^{6}	8.32×10^{6}	3.34×10^{11}	0.13	124.5	126.9
17 → **18**[b]	3.59×10^{5}	1.56×10^{6}	5.50×10^{6}	3.60×10^{11}	0.48	156.9	190.6
18 → **19**[b]	5.46×10^{10}	6.32×10^{10}	7.18×10^{10}	2.71×10^{11}	0.01	15.3	17.5
19 → **20** + H[b]	2.08×10^{9}	4.62×10^{9}	9.05×10^{9}	1.38×10^{11}	0.65	80.1	89.3

[a] In $cm^3\ s^{-1}molecule^{-1}$, with *T* in K and E_a in kJ/mol. [b] In s^{-1}, with *T* in K and E_a in kJ/mol. [c] This value includes a ZPVE correction calculated at the B3LYP level.

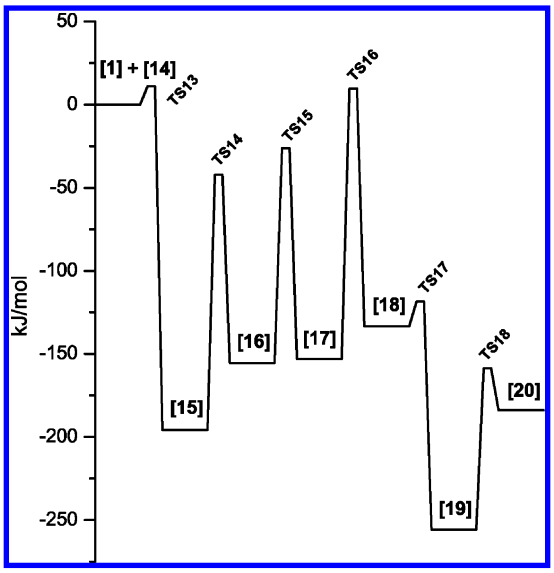

Figure 4. Formation of phenanthrene, C_6H_5 [**1**] + C_8H_6 [**14**] → $C_{14}H_{12}$ [**20**], calculated at the B3LYP/TZVP level.

BMK and recommend the latter for use in the mechanisms on which pyrolysis simulations such as those of Norinaga and Deutschmann are based.[13,14]

B. Formation of Phenanthrene. In Table 3, we provide the reaction rates obtained from TST for all of the steps of the reaction (cf. Figures 4 and 5) in the temperature range 300−1300 K, along with the fitted Arrhenius parameters *A* and *n* and computed values of E_a (including ZPVE). Not only for the formation of naphthalene but also for the formation of phenanthrene, we recommend the BMK activation energies for modeling purposes.

In the case of vinylacetylene, the phenyl radical can be added to both ends of the molecule, but in the case of phenylacetylene, the phenyl can only react with the triple bond. The addition of the phenyl radical is followed by a 1,4 hydrogen shift to yield the trans isomer [**16**], which isomerizes to the cis isomer [**18**] via the four-membered ring intermediate [**17**]. The electronic energy of the transition structure TS16 (10 kJ/mol, cf. Figure 4) lies just below the barrier (TS13, 11 kJ/mol) of the first, bimolecular reaction step. A new six-membered ring is formed in [**18**] to give phenanthrene [**20**].

C. Four-Membered Ring Intermediates. The radicalic intermediates [**11**] and [**17**] with a four-membered ring play a key role in the proposed reaction mechanisms for the formations of naphthalene and phenanthrene from reactions of phenyl with vinylacetylene and phenylacetylene, respectively. Unfortunately, we observe large discrepancies between the B3LYP and BMK results for the barriers between the four-membered ring intermediates and the cis isomers. For example, the BMK barrier (177.3 kJ/mol, including ZPVE) for the step [**11**] → [**12**] is more than 30 kJ/mol higher than the corresponding B3LYP barrier (145.7 kJ/mol, cf. Table 2). Also for the formation of phenanthrene, the BMK barrier (190.6 kJ/mol) for the step [**17**] → [**18**] is more than 30 kJ/mol higher than the corresponding B3LYP barrier (156.9 kJ/mol, cf. Table 3).

Similar data for the functionals BP86, BLYP, TPSS, TPSSh, and B97-K are collected in Table 4, showing that it is mainly the energy of the intermediates [**11**] and [**17**] that causes the large variations in computed activation energies for the [**11**] → [**12**] and [**17**] → [**18**] steps.

In an attempt to understand the different behavior of various exchange-correlation functionals, we have investigated the isomerization of the penta-1,3-dien-1-yl radical [**21**] as a model system (cf. Figure 6). For this model system, we have performed single-point RCCSD(T)(FC) calculations at the B3LYP/TZVP geometries with a restricted open-shell Hartree−Fock reference state (ROHF) using the correlation-consistent cc-pVTZ basis. According to the T1 diagnostic criteria,[47] the RCCSD(T) results do not suffer from a strong multireference character and represent a reliable set of reference data. The equilibrium and transition structures were determined at the B3LYP/TZVP level (Figure 6), and the results from various single-point calculations are shown in

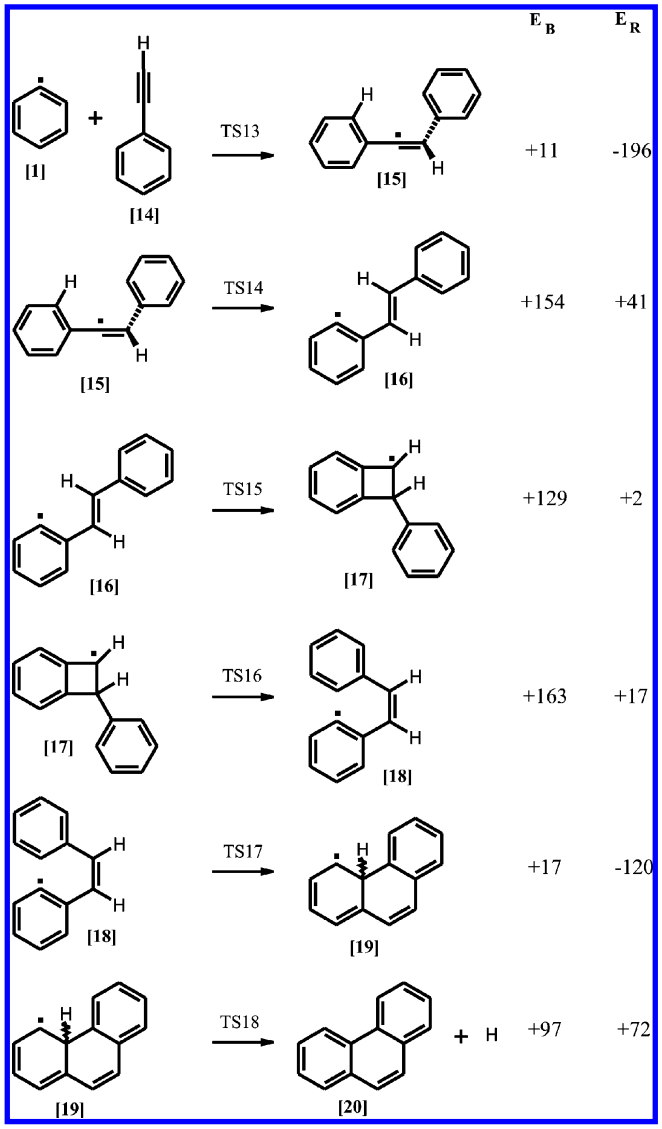

Figure 5. Intermediates and transition states on the reaction path (Figure 4) toward the formation of phenanthrene, C_6H_5 [**1**] + C_8H_6 [**14**] → $C_{14}H_{12}$ [**20**], calculated at the B3LYP/TZVP level (electronic energies in kJ/mol).

Table 4. Calculated (in the TZVP Basis) Relative Energies (in kJ/mol, with Respect To [**10**] and [**16**], Respectively) for the Formation of the Four-Membered Ring Intermediates [**11**] and [**17**] at the B3LYP/TZVP Geometries

method	TS9	[**11**]	TS10	TS15	[**17**]	TS16
BP86	122	−1	141	111	−8	146
BLYP	129	18	149	118	11	154
TPSS	125	0	144	115	−7	149
B3LYP	140	9	160	129	2	165
TPSSh	130	−4	149	119	−11	154
B97-K	142	−10	162	132	−16	169
BMK	141	−21	162	132	−29	168

Table 5. All of the DFT and coupled-cluster calculations indicate that the energy of the four-membered ring seems to be the most difficult to compute accurately. For the four-membered ring [**22**], the deviations of the results from the ROHF-CCSD(T)(FC) results vary between 51 (ROHF) and −40 kJ/mol [UHF-UMP2(FC)]. The corresponding deviations of the B3LYP (14 kJ/mol) and BMK (−16 kJ/mol) results are not so large but have different signs.

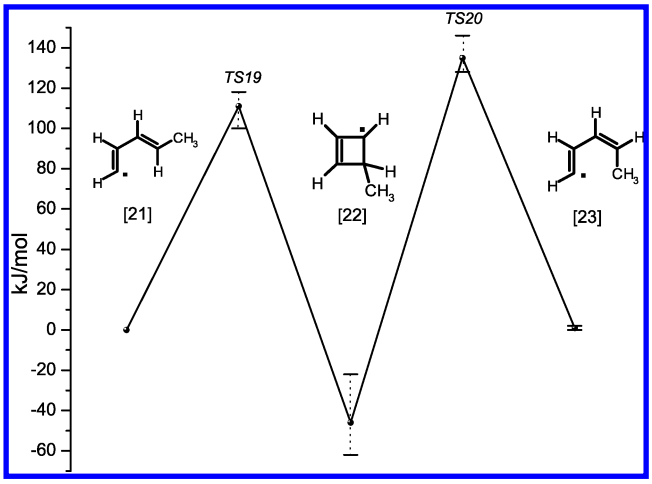

Figure 6. Energy profile of the isomerization of penta-1,3-dien-1-yl [**21**], see Table 5). The range of calculated DFT energies is indicated by error bars.

Table 5. Calculated (in the TZVP Basis) Relative Energies (in kJ/mol, with Respect To [**21**]) of the Model Reaction with Penta-1,3-dien-1-yl (cf. Figure 6) at the B3LYP/TZVP Geometries[a]

method	TS19	δ_{TS19}[b]	[**22**]	$\delta_{[22]}$[b]	TS20	δ_{TS20}[b]	[**23**]	$\delta_{[23]}$[b]
BP86	100	−11	−43	3	128	−7	0	−1
BLYP	110	−1	−22	24	136	1	2	1
TPSS	102	−9	−45	1	128	−7	1	0
B3LYP	117	6	−32	14	145	10	2	1
TPSSh	105	−6	−49	−3	132	−3	1	0
B97-K	118	7	−49	−3	146	11	2	1
BMK	116	5	−62	−16	144	9	0	−1
ROHF	182	71	5	51	211	76	6	5
UHF	137	26	−15	31	155	20	7	6
ROHF-UMP2(FC)	103	−8	−65	−19	129	−6	1	0
UHF-UMP2(FC)	124	13	−86	−40	152	17	0	−1
ROHF-UCC2(FC)	100	−11	−54	−8	124	−11	0	−1
UHF-UCC2(FC)	115	4	−67	−21	143	8	0	−1
ROHF-RCCSD(T)(FC)	111	0	−46	0	135	0	1	0

[a] A cc-pVTZ basis was used for the ROHF-RCCSD(T)(FC) calculations. [b] Deviation from the ROHF−RCCSD(T)(FC) result.

Spin contamination of the doublet states may be a reason for the differences between the DFT results. Indeed, the spin-unrestricted Hartree−Fock (UHF) expectation values of $\hat{S}^2$ amount to 1.30, 0.97, and 1.28 for the minima [**21**], [**22**], and [**23**], respectively, and as much as 1.45 and 1.53 for the transitions structures TS19 and TS20. The UHF and UHF-based values seem unreliable. On the other hand, all of the DFT values are much closer to 0.75 and are in good mutual agreement. For all of the minima, the DFT values range from 0.76 to 0.78 for all of the functionals studied, and the values for TS19 and TS20 vary between 0.77 and 0.81 and between 0.77 and 0.83, respectively. Overall, the DFT values agree to within 25 kJ/mol with the ROHF-CCSD(T)(FC) results, as can be seen from the error bars in Figure 6.

IV. Conclusions

We have proposed three reaction pathways for PAH growth from reactions of either vinyl- or phenylacetylene with a phenyl radical. We have found pathways via four-membered ring intermediates that enable a cis−trans isomerization. These intermediates have so far not been investigated in the literature.

Arrhenius parameters (pre-exponential A, temperature exponent n, and activation energy E_a) have been derived for all of the reaction steps on the three different pathways. We suggest the use of Arrhenius-like rate expressions such as eq 6 with our parameters for the first bimolecular steps in the kinetic modeling of refs 13 and 14.

Acknowledgment. This work was conducted in the Sonderforschungsbereich (SFB) 551 "Carbon from the Gas Phase: Elementary Reactions, Structures, Materials", which is funded by the Deutsche Forschungsgemeinschaft (DFG). We gratefully acknowledge the Fonds der Chemischen Industrie for additional financial support. We thank O. Deutschmann, K. Norinaga, and M. Olzmann for many fruitful discussions.

References

(1) Hüttinger, K. J. *Chem. Vap. Deposition* **1998**, *4*, 151.

(2) Hüttinger, K. J. In *Fibers and Composites*; Delhaès, P., Ed.; Taylor & Francis: Oxford, U. K., 2003; p 75.

(3) Becker, A.; Hüttinger, K. J. *Carbon* **1998**, *36*, 177.

(4) Norinaga, K.; Deutschmann, O.; Hüttinger, K. J. *Carbon* **2006**, *44*, 1790.

(5) Frenklach, M. *Phys. Chem. Chem. Phys.* **2002**, *4*, 2028.

(6) Richter, H.; Howard, J. B. *Phys. Chem. Chem. Phys.* **2002**, *4*, 2038.

(7) Klippenstein, S. J.; Miller, J. A. *J. Phys. Chem. A* **2005**, *109*, 4285.

(8) Appel, J.; Bockhorn, H.; Frenklach, M. *Combust. Flame* **2000**, *121*, 122.

(9) Moriarty, N. W.; Frenklach, M. *Proc. Combust. Inst.* **2000**, *28*, 2563.

(10) Bauschlicher, C. W., Jr.; Ricca, A. *Chem. Phys. Lett.* **2000**, *326*, 283.

(11) Frenklach, M.; Wang, H. *Proc. Combust. Inst.* **1991**, *23*, 1559.

(12) Kislov, V. V.; Mebel, A. M.; Lin, S. H. *J. Phys. Chem. A* **2002**, *106*, 6171.

(13) Norinaga, K.; Deutschmann, O. *Carbon* **2006**, submitted.

(14) Norinaga, K.; Deutschmann, O. In *Proceedings of the 15th European Conference on Chemical Vapor Deposition*; Electrochemical Society Proceedings: Pennington, NJ, 2005; Vol. 2005-09, p 348.

(15) *Turbomole*, v. 5.8; Cosmologic GmbH & Co.: Leverkusen, Germany, 2005. www.turbomole.com (accessed Nov 2006).

(16) Ahlrichs, R.; Bär, M.; Häser, M.; Horn, H.; Kölmel, C. *Chem. Phys. Lett.* **1989**, *162*, 165.

(17) Häser, M.; Ahlrichs, R. *J. Comput. Chem.* **1989**, *10*, 104.

(18) Treutler, O.; Ahlrichs, R. *J. Chem. Phys.* **1995**, *102*, 346.

(19) Schäfer, A.; Horn, H.; Ahlrichs, R. *J. Chem. Phys.* **1992**, *97*, 2571.

(20) All basis sets and auxiliary basis sets are available from ftp://ftp.chemie.uni-karlsruhe.de/pub (accessed Nov 2006).

(21) Vosko, S. H.; Wilk, L.; Nusair, M. *Can. J. Phys.* **1980**, *59*, 1200.

(22) Becke, A. D. *Phys. Rev. A: At., Mol., Opt. Phys.* **1988**, *38*, 3098.

(23) Perdew, J. P. *Phys. Rev. B: Condens. Matter Mater. Phys.* **1986**, *33*, 8822.

(24) Eichkorn, K.; Treutler, O.; Öhm, H.; Häser, M.; Ahlrichs, R. *Chem. Phys. Lett.* **1995**, *240*, 283.

(25) Eichkorn, K.; Treutler, O.; Öhm, H.; Häser, M.; Ahlrichs, R. *Chem. Phys. Lett.* **1995**, *242*, 625.

(26) Schäfer, A.; Huber, C.; Ahlrichs, R. *J. Chem. Phys.* **1994**, *100*, 5829.

(27) Becke, A. D. *J. Chem. Phys.* **1993**, *98*, 5648.

(28) Lee, C.; Yang, W.; Parr, R. G. *Phys. Rev. B: Condens. Matter Mater. Phys.* **1988**, *37*, 785.

(29) Boese, A. D.; Martin, J. M. L. *J. Chem. Phys.* **2004**, *121*, 3405.

(30) Von Arnim, M.; Ahlrichs, R. *J. Chem. Phys.* **1999**, *111*, 9183.

(31) Helgaker, T. *Chem. Phys. Lett.* **1991**, *182*, 503.

(32) Deglmann, P.; Furche, F.; Ahlrichs, R. *Chem. Phys. Lett.* **2002**, *362*, 511.

(33) Deglmann, P.; Furche, F. *J. Chem. Phys.* **2002**, *117*, 9535.

(34) Steinfield, J. I.; Francisco, J. S.; Hase, W. L. *Chemical Kinetics and Dynamics*, 2nd ed.; Prentice Hall: New York, 1999.

(35) Carissan, Y.; Klopper, W. *ChemPhysChem* **2006**, *7*, 1770.

(36) Perdew, J. P.; Wang, Y. *Phys. Rev. B: Condens. Matter Mater. Phys.* **1992**, *45*, 13244.

(37) Tao, J.; Perdew, J .P.; Staroverov, V. N.; Scuseria, G. E. *Phys. Rev. Lett.* **2003**, *91*, 146401.

(38) Staroverov, V. N.; Scuseria, G. E.; Perdew, J. P.; Tao, J. *J. Chem. Phys.* **2003**, *119*, 12129.

(39) Weigend, F.; Häser. M. *Theor. Chem. Acc.* **1997**, *97*, 331.

(40) Hättig, C.; Weigend, F. *J. Chem. Phys.* **2000**, *113*, 5154.

(41) Knowles, P. J.; Hampel, C.; Werner, H.-J. *J. Chem. Phys.* **1993**, *99*, 5219.

(42) Knowles, P. J.; Hampel, C.; Werner, H.-J. *J. Chem. Phys.* **2000**, *112*, 3106.

(43) Watts, J. D.; Gauss, J.; Bartlett, R. J. *J. Chem. Phys.* **1993**, *98*, 8718.

(44) Werner, H.-J.; Knowles, P. J.; Lindh, R.; Manby, F. R.; Schütz, M.; Celani, P.; Korona, T.; Rauhut, G.; Amos, R.D.; Bernhardsson, A.; Berning, A.; Cooper, D. L.; Deegan, M. J. O.; Dobbyn, A. J.; Eckert, F.; Hampel, C.; Hetzer, G.; Lloyd, A. W.; McNicholas, S. J.; Meyer, W.; Mura, M. E.; Nicklaβ, A.; Palmierir, P.; Pitzer, R.; Schumann, U.; Stoll, H.; Stone, A. J.; Tarroni, R.; Thorsteinsson, T. *Molpro*, version 2002.6; University College Cardiff Consultants Limited: Wales, U. K., 2003. See http://www.molpro.net (accessed Nov 2006).

(45) Lindh, R.; Ryu, U.; Liu, B. *J. Chem. Phys.* **1991**, *95*, 5889.

(46) Hampel, C.; Peterson, K. A.; Werner, H.-J. *Chem. Phys. Lett.* **1992**, *190*, 1.

(47) Lee, T. J.; Taylor, P. R. *Int. J. Quantum Chem.* **1989**, *S23*, 199.

CT600255U